Preprint Title	Supramolecular Assemblies of Donor-Acceptor Stenhouse Adduct Amphiphiles as Macroscopic Soft Scaffolds
Authors	Ka-Lung Hung, Leong-Hung Cheung, Yikun Ren, Ming-Hin Chau, Yan-Yi Lam, Takashi Kajitani and Franco King-Chi Leung
Publication Date	17 Apr. 2024
Article Type	Full Research Paper
Supporting Information File 1	Cover Letter-DAn.pdf; 305.9 KB
Supporting Information File 2	Movie S1-DA 11.mp4; 56.4 MB
Supporting Information File 3	Movie S2-DA 7.mp4; 45.6 MB
Supporting Information File 4	Movie S3-DA 6.mp4; 46.5 MB
Supporting Information File 5	SI-DAn.pdf; 4.7 MB
ORCID® iDs	Ka-Lung Hung - https://orcid.org/0009-0001-5604-426X; Leong-Hung Cheung - https://orcid.org/0000-0001-5959-0613; Ming-Hin Chau - https://orcid.org/0000-0003-1747-8521; Franco King-Chi Leung - https://orcid.org/0000-0003-0895-9307

Supramolecular Assemblies of Donor-Acceptor Stenhouse Adduct Amphiphiles as Macroscopic Soft Scaffolds

Ka-Lung Hung [a,b], Leong-Hung Cheung [b], Yikun Ren [a,b], Ming-Hin Chau [b], Yan-Yi Lam [b], Takashi Kajitani [c], and Franco King-Chi Leung[a,b,d,*]

[a] The Hong Kong Polytechnic University Shenzhen Research Institute, Shenzhen 518057, China.
[b] State Key Laboratory of Chemical Biology and Drug Discovery, Department of Applied Biology and Chemical Technology, The Hong Kong Polytechnic University, Hong Kong, China.
[c] Open Facility Development Office, Open Facility Center, Tokyo Institute of Technology, 4259 Nagatsuta, Midori-ku, Yokohama 226-8503, Japan.
[d] Centre for Eye and Vision Research, 17W Hong Kong Science Park, Hong Kong, China.

Email: Dr. Franco King-Chi Leung – kingchifranco.leung@polyu.edu.hk

* Corresponding author

Abstract

Designing photo-harvesting and photoresponsive supramolecular systems in aqueous media, the fabrication of photoswitch as an amphiphilic structure enables non-invasive functional response by photoirradiation. Although most of aqueous supramolecular assemblies across multiple length-scale were driven by high-energy and bio-damaging UV-light, previously we reported donor-acceptor Stenhouse adduct (DASA) amphiphile controlled by while-light.

Herein, we present a series of DASA amphiphiles with minor structural modifications on the chain length of alkyl-linker, which connect DASA motif with hydrophilic part. The excellent photoswitchabilities in organic media and photoresponsiveness in aqueous media, driven by visible-light, are revealed with UV-vis absorption spectroscopy. The supramolecular structures are confirmed by electronic microscopies across multiple length-scale, while the supramolecular packing structures at macroscopic length-scale are revealed with X-ray diffraction. Driven by visible-light irradiation, the large geometrical transformations of DASA amphiphiles enable supramolecular transformation at microscopic length-scale, and subsequently disassemble the macroscopic soft scaffolds of DASA amphiphiles. The results indicate the feasibility in developing visible-light controlled macroscopic scaffolds for offering opportunity in fabricating biomedical materials with visible-light controlled microenvironment and future soft robotic systems.

Keywords

Donor-Acceptor Stenhouse Adduct; Supramolecular Transformation; Photoresponsive Molecular Amphiphile; Visible-Light

Introduction

Solar energy is of paramount importance to life-forms on the earth for various vital parameters, such as, maintaining stable temperature and enabling photosynthesis as the basis of food chain. Inspired by the natural photosynthesis processes in harnessing light energy, the synthetic molecules, serving as the counterpart to natural systems, were designed and functionalized with photoresponsive and photo-absorbing functional motifs, in harvesting light energy for smart materials, *e.g.*, solar cell, photosensitizer, photochromic material[1-4]. Supramolecular assembly is commonly found in natural systems to serve different biological functions in

precise manners, *e.g.*, actin in biological molecular motor, cytoskeleton, and cell membrane[5-8]. Mimicking natural supramolecular assemblies in aqueous media, the intrinsic supramolecular dynamicity, stimuli-responsiveness, and molecular functional tunability of synthetic supramolecular systems are precisely controlled with the delicate organic molecular design and synthesis[9-14]. Synthetic supramolecular systems have recently advanced to respond various external stimulations, *e.g.*, light, pH, organic solvents, ions, and heat[15-22]. Light enables non-invasive stimulation with high spatial and temporal precision for controlling supramolecular assembly structures in organic and aqueous media[19, 23-26]. Various photochromic and photoresponsive moieties, such as, stiff-stilbene[27], azobenzene[28, 29], molecular motor[19, 30, 31], spiropyran[32-34], indigo[35, 36], and donor-acceptor Stenhouse adduct,[37, 38] have been equipped as photoswitchable supramolecular systems for smart functions in electronic, optoelectronic, and biomedical materials[31, 39-41].

Photoresponsive molecular amphiphiles have been demonstrated with their supramolecular responsiveness, complexity, and adaptability in aqueous media[42-44]. Supramolecular assembly systems of photoresponsive molecular amphiphiles in aqueous media have significantly advanced the resulting assembly transformations either in solution or at air-water interface, and even sustained artificial muscle-like functions[17, 44, 45]. To tackle poor biocompatibility observed in supramolecular assemblies of UV-driven photoresponsive molecular amphiphiles, visible-light driven supramolecular systems enabled supramolecular transformations at multiple length-scales are urgently required. Some visible-light driven supramolecular assembled systems at microscopic length-scale, such as spiropyrans, azobenzenes, indigos, have been reported with controlled supramolecular assembly transformations in aqueous media[28, 36, 46, 47], however, very limited visible-light driven supramolecular transformation at macroscopic length-scale were reported. Pioneered by Leung and Feringa on UV driven supramolecular transformation at macroscopic length-scale[43, 44],

we recently reported the first indigo amphiphiles in fabrication of macroscopic soft scaffolds with photo-shrinking property as cell-material interface[35].

Alternatively, donor-acceptor Stenhouse adducts (DASA) was firstly reported by Read de Alaniz as new class of photoswitch[48, 49]. The intrinsic large geometrical structural transformation from *open*-isomer to *cyclized*-isomer and simple modular synthesis of DASA enable various applications in photochromic systems and smart functional materials[48, 50-60]. We reported the first DASA amphiphiles (DA) assembled into large aspect-ratio nanostructures in aqueous media and sustained supramolecular structural transformations, controlled by white-light[38]. The large aspect-ratio nanostructures of DAs were fabricated into macroscopic soft scaffolds with white-light controlled disassembling processes. Furthermore, the red-light responsiveness of DA could be regained in aqueous media upon co-assembly with stiff-stilbene amphiphile, due to reduced intermolecular stacking of DA[37]. With the excellent photoresponsiveness of DAs at multiple length-scale, it significantly increases the urgency in investigating the corresponding biocompatibility and molecular structural derivatives. On the basis of the molecular design of the reported DA, we design and synthesize, featured with second generation DASA switching motif, a series of DA with different chain length of the alkyl-linker (**DA$_n$**), which connects indoline motif of DASA with the hydrophilic part (carboxylic acid motif) (Scheme 1). The alkyl-linker length allows fine adjustment of the hydrophobic volume of **DA$_n$**, enabling significant packing parameters change upon assembling in aqueous media. At microscopic length-scale, the expected supramolecular assembly and the related assembly transformations can be controlled systematically by visible light irradiation. At macroscopic length-scale, the macroscopic soft scaffolds of **DA$_n$** are able to perform macroscopic structure disassembling upon visible-light irradiation. The biocompatibility of macroscopic soft scaffolds of **DA$_n$** are investigated with limited cytotoxicity. The current work

could open up new prospects in developing biomedical materials with visible-light controlled microenvironment and future soft robotic systems.

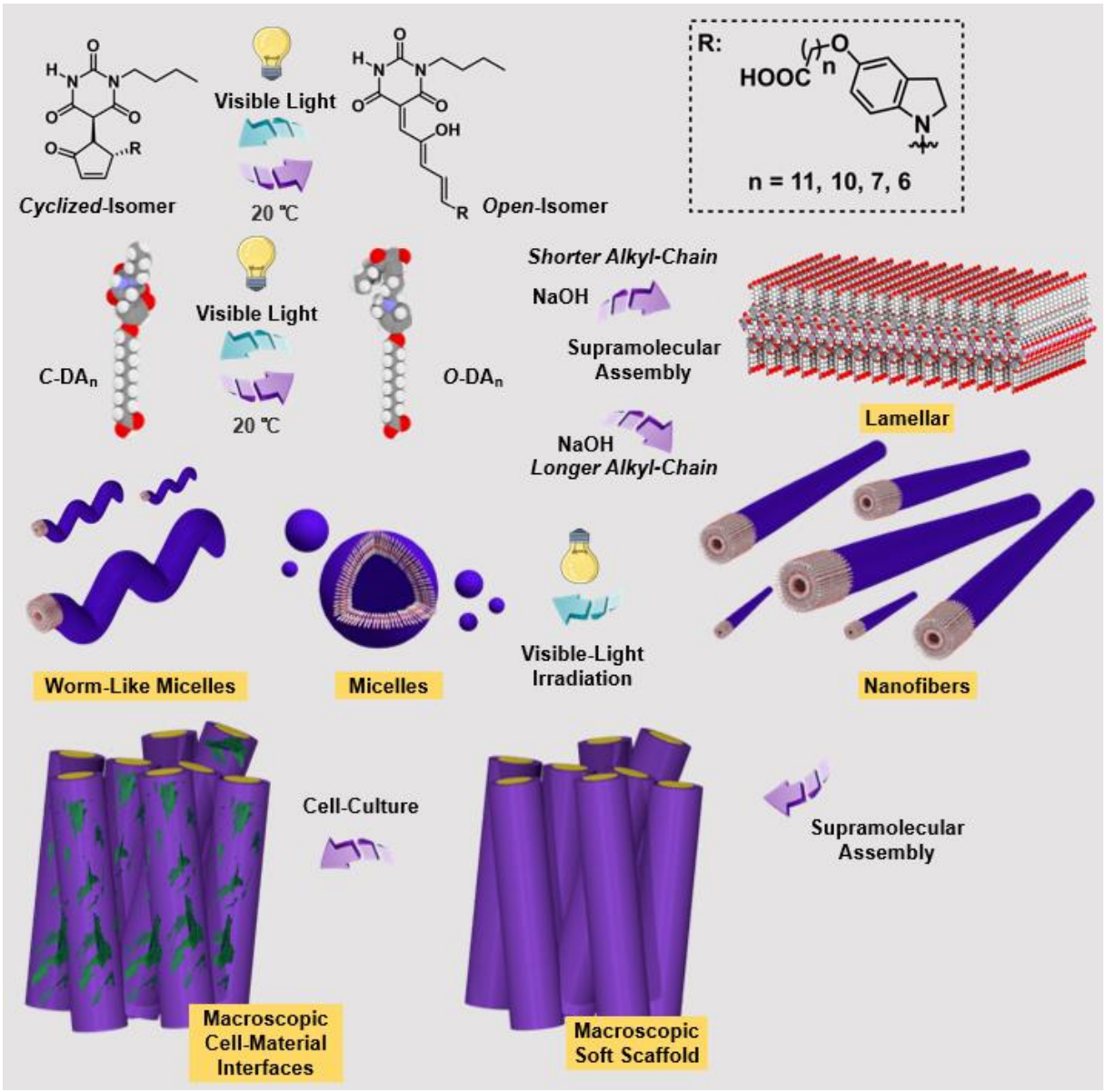

Scheme 1. Schematic illustration of the reversible visible-light controlled ring-closure and thermal driven ring-opening processes of **DA$_n$** and supramolecular assembly across length-scales

Results and Discussion

Synthesis and Design of Donor-Acceptor Stenhouse Adduct Amphiphile (DA)

We designed and synthesized a series of **DA$_n$** with different chain length of the alkyl-linker, *i.e.*, chain length = 11, 7, and 6, affording **DA$_{11}$**, **DA$_7$**, and **DA$_6$**, respectively. The resulting chain length effect of the alkyl-linkers of **DA$_{11}$**, **DA$_7$**, and **DA$_6$** is discussed with our previously reported **DA$_{10}$**.[38] The donor parts of **DA$_n$** were synthesized by alkylation in the presence of K_2CO_3 under nitrogen and followed by reduction of indole motif of the compound **1$_n$** into indoline (compound **2$_n$**). The obtained compound **2$_n$** was deprotected under basic conditions (Scheme 2). **DA$_n$** with different chain-length of alkyl-linkers were synthesized through an aza-Piancatalli rearrangement with a barbiturate furan adduct (compound **4**) and compound **3$_n$** motif under ambient condition in dichloromethane. (Scheme 2). The synthesis and characterization of all newly designed compounds, including **DA$_{11}$**, **DA$_7$**, and **DA$_6$**, were summarized in the supporting information (Figure S12–S32).

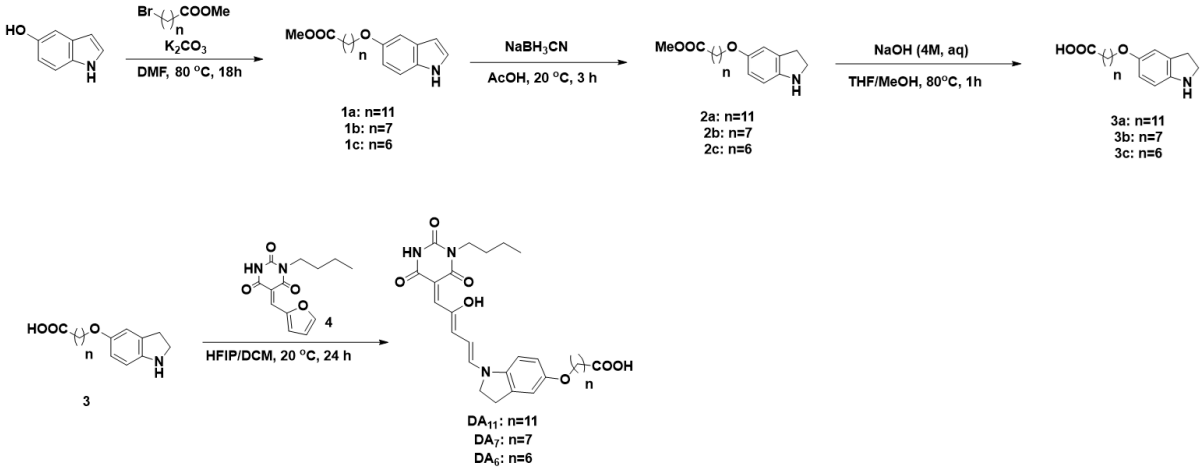

Scheme 2: Synthetic Pathway of **DA$_n$**

Photochemical Properties of DA_n in Organic Media

The photochemical properties of **DA_n** were firstly studied in organic solvent by UV-vis absorption spectroscopy. The synthetically prepared **DA_{11}** (20 μM) in THF solution shows a strong absorption band at 470–685 nm in the UV-vis absorption spectrum (Figure 1a). Upon 625 nm red-light irradiation for 60 s at 20 °C, the strong absorption band was diminished at 470–685 nm with a clear isosbestic point at 259 nm to reach the photostationary state (PSS, Figure 1a, red-line), which indicates a selective photoisomerization process from *O*-**DA_{11}** (*open*-isomer) (Figure 1a, black-line and blue-line) to *C*-**DA_{11}** (*cyclized*-isomer) (Figure 1a, red-line). The resulting solution was continued to irradiate with 625 nm red-light for 60 s at 20 °C and store in dark for thermal back reaction at 20 °C for 60 min subsequently to test the reversibility and photostability in organic solvent (Figure S1a and S1b). The photoisomerization between *O*-**DA_{11}** and *C*-**DA_{11}**, upon 625 nm irradiation red-light and thermal back reaction in the dark, could be repeated over 5 cycles with only 5% absorbance decreases per cycle (Figure S1a and S1b), while comparing to the previous studied of photoswitching cycles of **DA_{10}** was observed as 10% absorbance decreases per cycle,[38] indicating a mild improvement of fatigue resistant for **DA_{11}**.

To further investigate the photostability and reversibility of other **DA_n**, the **DA_n** with shorter alkyl-linkers were also synthesized and observed in THF solvent by UV-vis absorption spectroscopy, where they performed similar photophysical properties to that of observed in **DA_{11}** (Figure 1a). Both **DA_7** and **DA_6** show a strong absorption band at 470–685 nm in UV-vis absorption spectra (Figure 1b and 1c). Upon red-light 625 nm irradiation for 60 s at 20 °C, the strong absorption band was diminished, as same as **DA_{11}**, at 470–685 nm with clear isosbestic point at 259 nm to reach PSS (Figure 1b and 1c, red-line). After thermal back reaction in dark at 20 °C for 60 min (Figure 1b and 1c, blue-line), the strong absorption band was recovered and indicated a selective photoisomerization process from *open*-isomers (*O*-**DA_7** and *O*-**DA_6**)

(Figure 1b and 1c, black-line and blue-line) to *cyclized*-isomers (*C*-**DA$_7$** and *C*-**DA$_6$**) (Figure 1a and 1c, red-line). The results showed the feasibility of photo-reversibility of **DA$_7$** and **DA$_6$** in five photoswitching cycles, however, more significant fatigue effect was observed in both **DA$_7$** (Figure S1c and S1d) and **DA$_6$** (Figure S1e and S1f) with 15% absorbance declines per cycle. The more obvious fatigue effects were observed in the photoisomerizations of **DA$_7$** and **DA$_6$**, it might be attributed to a stabilization effect through hydrogen bonding and the favored *cyclized*-isomer in polar solvents. The increased alkyl-linker lengths of **DA$_{10}$** and **DA$_{11}$** enabled improved photostability than that of observed in **DA$_7$** and **DA$_6$**, possibly due to the reduced stabilization effect of *cyclized*-isomer in polar environment, which improve fatigue resistant of **DA$_n$** in polar environment.

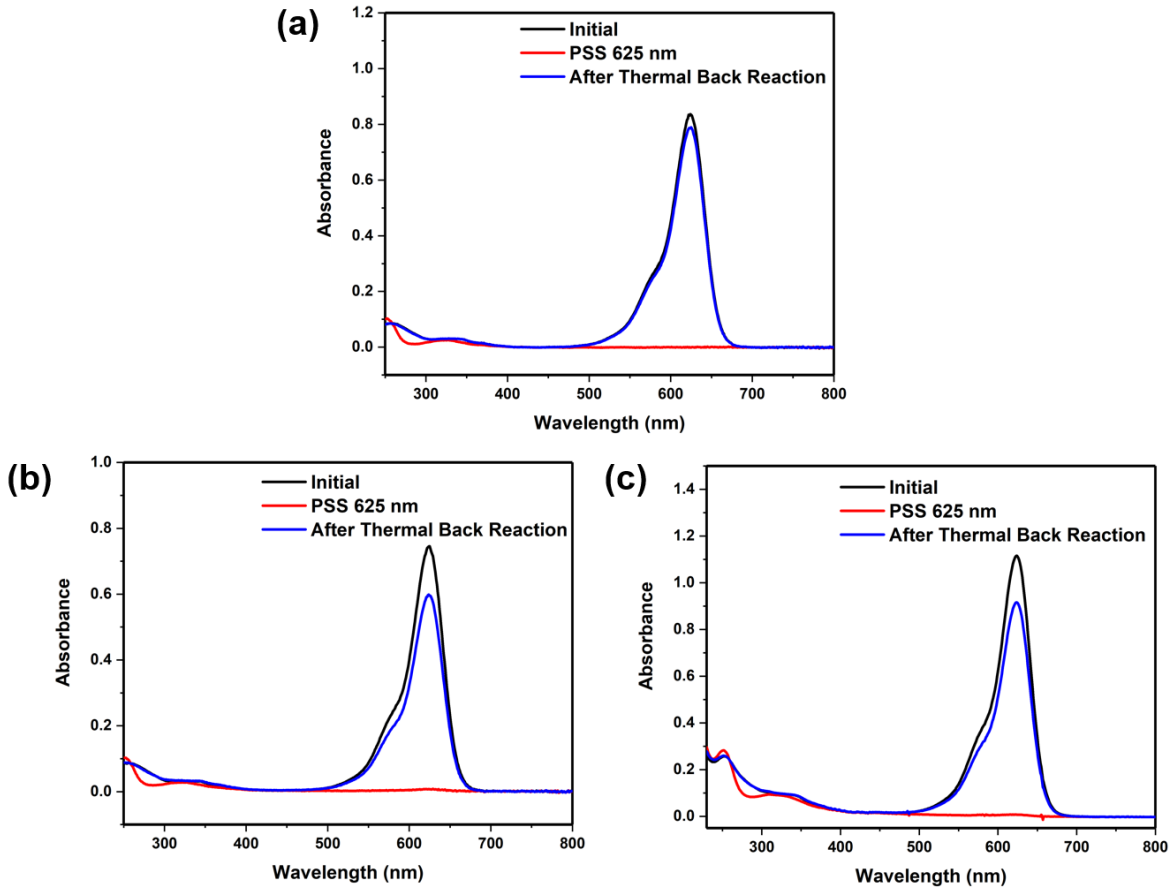

Figure 1. UV-vis absorption spectral changes of (a) **DA$_{11}$**, (b) **DA$_7$**, (c) **DA$_6$**, in THF solution (20 μM) at initial (black-line), upon 625 nm irradiation over 1 min (red-line) and Thermal back reaction at 20 °C over 60 min (blue-line). Irradiation of UV-vis sample was carried out at 20 °C

using a Thorlabs model M625F2 high-power LED (625 nm, 1.0 A) positioned at a distance of 1 cm from the sample.

Photochemical Properties of DA_n in Aqueous Media

Due to the well-performed photoswitchabilities of **DA_n** in organic solvent, the photochemical properties and their supramolecular assembly structures were investigated in aqueous media. An aqueous solution of **DA_{11}** was prepared as 5.0 weight % (wt.%) in MilliQ water and followed by deprotonation with 1.0 equivalent of NaOH, showing excellent aqueous solubility up to 93 mM as a deep purple solution. An aqueous solution of **DA_{11}** (43 μM), diluted from the stock solution (5.0 wt.%), was investigated in UV-vis absorption spectroscopy. Absorption bands at 250–325 nm and 430–800 nm was observed (Figure 2a), where the absorption maximum located at 667 nm accompanied with a shoulder peak at 561 nm, which is similar to that of observed in **DA_{10}**[38]. The significant spectral shift and peaks broadening of **DA_{11}** were observed compared to THF solvent (Figure 2a, black-line), possibly due to its supramolecular assembly formation in aqueous media. Because of the broadened absorption band of **DA_{11}** in aqueous media, the photoisomerization cannot be effectively driven by a narrow emission wavelength of 625 nm LED light source, which is similar as our previously studies[38]. Thus, a while-light source with broad emission wavelength was employed for driving photoisomerization of **DAs** in aqueous medium. The photoisomerization process of **DA_{11}** was induced upon white-light irradiation for 60 min at 20 °C, the absorption band at 430–800 nm was decreased, along with increased absorption band at 250–325 nm and clear isosbestic points at 286 nm, 357 nm and 443 nm (Figures 2a, S2a, red-line, S2b). The results indicated a slower selective photoisomerization process from *O*-**DA_{11}** and *C*-**DA_{11}** in aqueous media than that of observed in THF (Figure 1a). The resulting aqueous solution was further studied with its thermal back process, after photoisomerization from *O*-**DA_{11}** and *C*-**DA_{11}**, showing no reverse switching process to *O*-**DA_{11}** by storage in the dark at 20 °C (Figure S2b). Given that the

cyclized-isomers of common DASAs remained stable in aqueous media, which is irreversible for switching back to *open*-isomer of DASAs[48, 49, 61]. The hindered thermal back reaction of **DA$_{11}$** should also be attributed to similar phenomenon, which was observed in our previously reported **DA$_{10}$**[38].

The **DA$_n$** designs with shorter alkyl-linkers, *i.e.*, **DA$_7$** and **DA$_6$**, were also investigated with the identical preparation protocol as mentioned above. An aqueous solution of **DA$_7$** (43 μM) showed an absorption band at 250–325 nm and 430–800 nm (Figure 2b), where the absorption maximum located at 543 nm accompanied with a shoulder peak at 667 nm (Figure 2b). While an aqueous solution of **DA$_6$** (43 μM) with similar absorption band at 250–325 nm and 430–800 nm, the broad absorption peaks at 557 nm with a shoulder peak at 667 nm, but the maximum peak located at 263 nm (Figure 2c). Upon white-light irradiation for 60 min at 20 °C, the absorption band at 430–800 nm was decreased, observed in both **DA$_7$** and **DA$_6$**, where the absorption band at 250–470 nm was increased. The clear isosbestic points were located at 286 nm and 449 nm for **DA$_7$** (Figures 2b, S3a, red-line, S3b), while the isosbestic points were located 467 nm and 283 nm for **DA$_6$** (Figures 2c, S4a, red-line, S4b), indicating selective photoisomerization processes observed in both aqueous solutions of *O*-**DA$_7$** to *C*-**DA$_7$,** and *O*-**DA$_6$** to *C*-**DA$_6$**, respectively. No obvious thermal back process was observed in both **DA$_7$** and **DA$_6$**, which is similar to that of observed in **DA$_{11}$** and **DA$_{10}$.** The results indicated that the subtle alkyl-linker length modification can induce to obvious spectral shift, implying different supramolecular assemblies of **DA$_n$** in aqueous media.

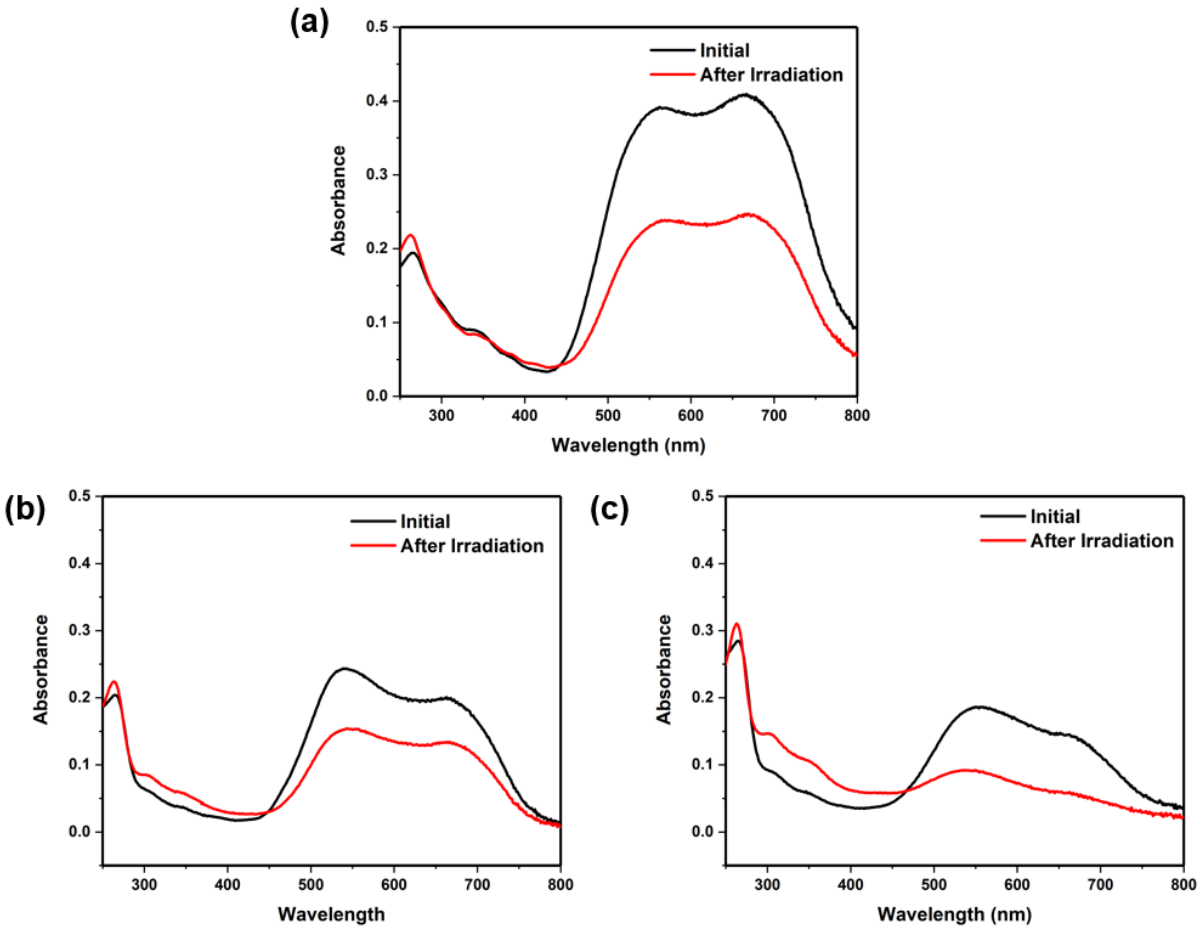

Figure 2. UV-vis absorption spectral changes of (a) **DA$_{11}$**, (b) **DA$_7$**, (c) **DA$_6$** in aqueous solution (43 μM) at 20 °C before irradiation (black), upon white light irradiation over 60 min (red). Irradiation of UV-vis samples was carried out at 20 °C using a light guide equipped BBZM-I xenon light source (380–800 nm, 300 W) positioned at a distance of 1 cm from the sample.

Photocontrolled Supramolecular Assemblies of DA$_n$ in Aqueous Media

A freshly prepared aqueous solution of **DA$_{11}$** (4.1 mM, 0.25 wt.%), in the presence of 1.0 equivalent of NaOH, was further diluted into a range of concentration from 1.0 x 10^{-4} to 0.1 mM for estimating the critical aggregation concentration (CAC) by using static light scattering (SLS). The CAC of the aqueous solution of **DA$_{11}$** was estimated as < 6.0 μM (Figure S5). To investigate the supramolecular assembly in microscopic length-scale, a freshly prepared aqueous solution of **DA$_{11}$** (5.0 wt.%, 82 mM) in the presence of 1.0 equivalent of NaOH, followed by diluting into 0.25 wt.% (4.1 mM) and imaged using negative-stained transmission

electron microscopy (TEM). The observed images show that **DA$_{11}$** assembled into a large-aspect-ratio of nanofibers with several hundred nanometers in length but bundled into ~100 nanometers in width (Figure 3a), which is similar to that of observed in **DA$_{10}$**. Upon white-light irradiation for 60 min at 20 °C, the photoisomerization of **DA$_{11}$** (4.1 mM) induced its supramolecular assembly transformation from bundled nanofibers into a mixture of worm-like micelles and micelles structures (diameter: 3 – 4 nm) (Figure 3b), which is similar to that of observed in **DA$_{10}$**.[38] The obtained results indicated that the subtle increased length of alkyl-linker in **DA$_{11}$** performed essentially identical to that of observed in **DA$_{10}$** at microscopic length-scale. Followed identical preparation protocol, aqueous solutions of **DA$_{7}$** (0.25 wt.%, 4.5 mM), and **DA$_{6}$** (0.25 wt.%, 4.6 mM) were prepared from dilution of 5 wt.% in the presence of 1.0 equivalent of NaOH, respectively. The CACs of aqueous solutions of **DA$_{7}$** and **DA$_{6}$** were estimated as < 0.05 mM (Figure S6) and < 0.1 mM (Figure S7), respectively. An aqueous solution of **DA$_{7}$** (0.25 wt.%) formed lamellar structure with ~ 200 nm in length and ~ 40 nm in width (Figure 3c), observed by TEM. A lamellar structure was observed in an aqueous solution of **DA$_{6}$** (Figure 3e). More significant supramolecular assembly structural variation was observed upon decreasing alkyl-linker from n = 11 to n = 7 or 6. Similarly, the lamellar structure of **DA$_{7}$** were disassembled into worm-like micellar structures (Figure 3d), upon white-light irradiation. The lamellar structure of **DA$_{6}$** remained unchanged (Figure 3f), possibly due to stability of the resulting supramolecular structures. The intrinsic photoswitchability and supramolecular assembly structural transformation at microscopic length-scale, it enables possibilities of **DA$_{n}$** applied for fabrications of macroscopic soft scaffolds after charge screening with complementary ions.

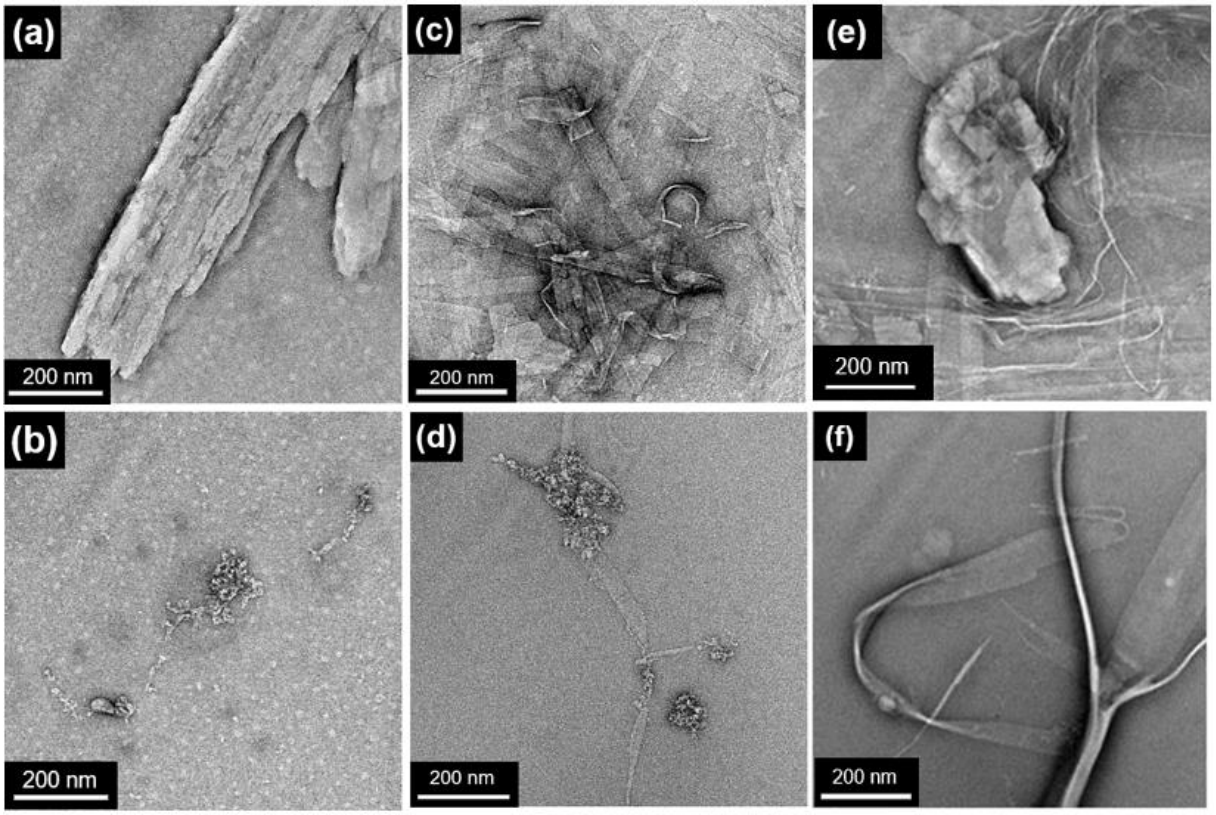

Figure 3. TEM images of freshly prepared aqueous solutions before irradiation of (a) **DA_{11}** at 0.25 wt.% (4.1 mM), (c) **DA_7** at 0.25 wt.% (4.5 mM) and (e) **DA_6** at 0.25 wt.% (4.6 mM). The solutions of (b) **DA_{11}**, (d) **DA_7**, (f) **DA_6** was irradiated with white-light irradiation over 60 min at 20 °C.

Fabrications and Characterizations of Macroscopic Soft Scaffolds of DA_n in Aqueous Media

A freshly prepared aqueous solution of **DA_{11}** (5.0 wt.%, 82 mM) gave a deep-blue and remained stable over months. The highly negative charged nanofibers of **DA_{11}** were supramolecular assembled into macroscopic soft scaffold by applying a shear-flow method to eject the solution of **DA_{11}** into a shallow pool of calcium chloride solution (150 mM) (Figure 4a). As demonstrated previously calcium ion provides a maximized binding affinity to carboxylate group of **DA_n**, which enables **DA_{11}** charge screening to stabilize the obtained macroscopic soft scaffold. Under optical microscopy, the macroscopic soft scaffold of **DA_{11}** was revealed as a deep-blue string with diameter ~ 560 μm (Figure S8), while no observable microscopic

structure was observed in the optical microscopic image with crossed polarizer (Figure S8). The intrinsic microscopic structure of the macroscopic soft scaffold of **DA$_{11}$** was investigated with scanning electron microscopy (SEM) and showed with partially aligned bundled nanofibers of **DA$_{11}$** to the long-axis of the macroscopic soft scaffold (Figure 4b). To provide detailed structural parameters and orientational order, *i.e.*, degree of alignment, of the macroscopic soft scaffold of **DA$_{11}$** were measured with through-view wide-angle X-ray diffraction (WAXD). In the 2D WAXD image of the **DA$_{11}$** macroscopic soft scaffold, prepared on a sapphire substrate at 20 °C and exposed to X-ray for 20 min, a diffraction ring is observed in the region of q = 0.5 – 5.0 nm^{-1} (Figure 4c), which is similar to that of observed in **DA$_{10}$**[38]. The angular dependency of the peak intensity of the diffraction ring, converted from the 2D WAXD image of **DA$_{11}$** macroscopic soft scaffold shows a pair of weak peak maxima with full-width half-maximum (fwhm) ~ 110° (Figure S9), while **DA$_{10}$** macroscopic soft scaffold showed no obvious peak maximum. The results indicated that subtle unidirectional alignment of bundled nanofibers of **DA$_{11}$** to the long-axis of **DA$_{11}$** macroscopic soft scaffold was revealed, while no significant unidirectional alignment was observed in **DA$_{10}$** macroscopic soft scaffold. The 1D WAXD pattern of **DA$_{11}$** macroscopic soft scaffold of the 2D WAXD image shows diffraction peaks at d = 2.24 nm and 0.36 nm (Figure 4d). The diffraction peak at d = 2.24 nm should be attributed to the diffraction originated from the longer molecular axis of **DA$_{11}$** in a dimeric form, while the d = 0.36 nm is originated from the π-π stacking of the DASA motif. Consistently, the diffraction from the longer molecular axis of **DA$_{10}$** in a dimeric form is shorter (d = 2.19 nm) than that of observed in **DA$_{11}$**, indicating that the subtle chain length variation of alkyl-linker of **DA$_n$** can be revealed even at macroscopic length-scale. To further verify this packing structure variation, the 2D WAXD images of **DA$_7$** and **DA$_6$** macroscopic soft scaffolds (Figure S10a and Figure S11a, respectively) show diffraction rings with d-spacings at 1.50 nm and 1.45 nm respectively (Figure S10b and Figure S11b), revealing the shortened longer molecular axis of both **DA$_7$** and **DA$_6$** in a dimeric form than that of observed in **DA$_{11}$** and **DA$_{10}$**. The major

observed diffraction peaks of **DA$_7$** and **DA$_6$** macroscopic soft scaffolds were also originated from the π-π stacking of the DASA motifs. However, there are no significant unidirectional alignment observed in both **DA$_7$** and **DA$_6$** macroscopic soft scaffolds in WAXD and SEM images (Figure S10a, S10c and Figure S11a, S11c, respectively). The electron microscopy and WAXD results revealed that longer chain length of alkyl-linkers of **DA$_n$** can slightly improve the degree of unidirectional alignment of nanostructures of **DA$_n$** in the corresponding macroscopic soft scaffolds, possibly due to the higher tendency nanostructure bundling with longer alkyl-linker.

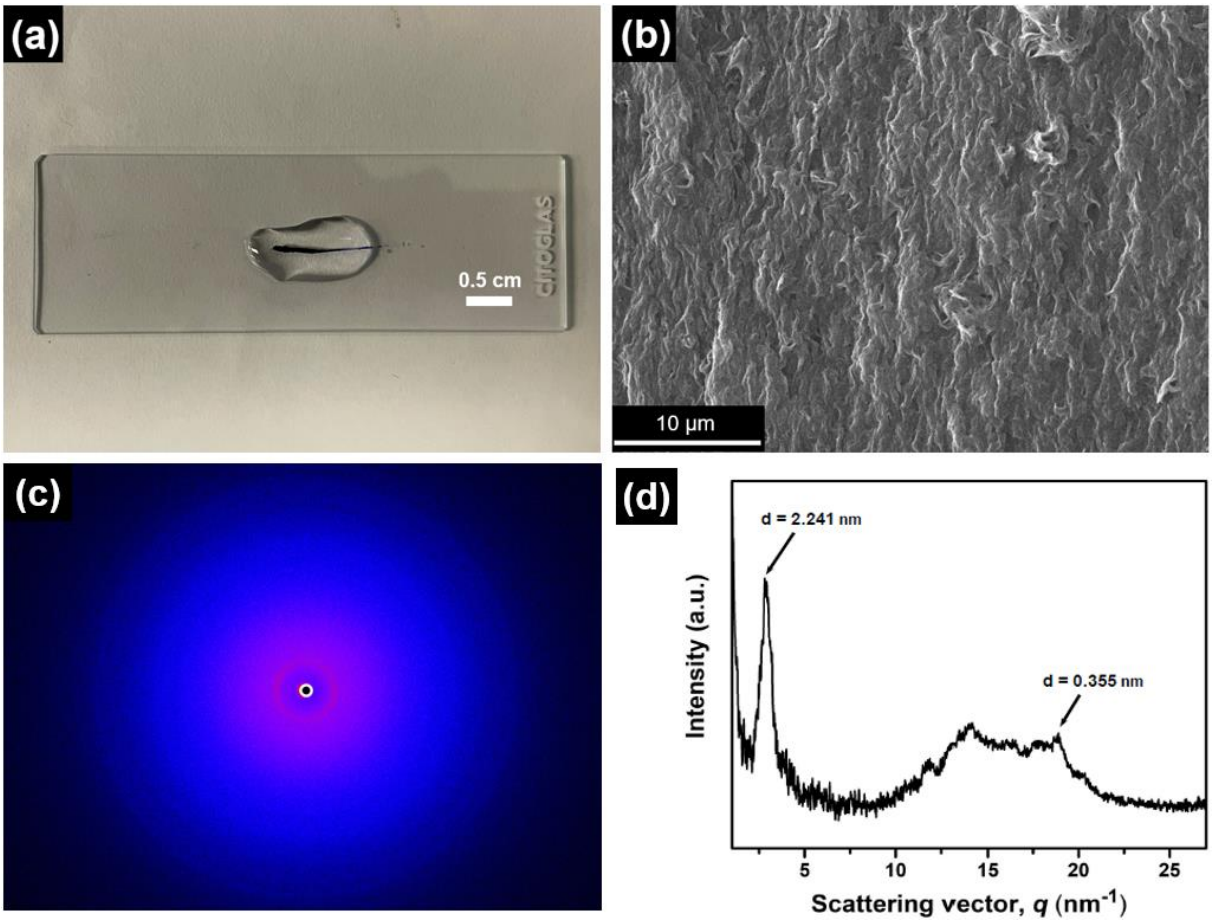

Figure 4. Photograph of aqueous solutions of **DA$_{11}$** freshly prepared (82.0 mM) was ejected into a shallow pool of $CaCl_2$ solution (150 mM). (b) SEM image of a macroscopic scaffold composed of **DA$_{11}$** prepared from a solution of $CaCl_2$ (150 mM). (c) 2D-WAXD image of **DA$_{11}$** macroscopic soft scaffold with 20 min X-ray exposure time. (d) 1D-WAXD pattern of **DA$_{11}$** macroscopic soft scaffold of 2D WAXD image in (c).

Photocontrolled Disassembly and Biocompatibility of Macroscopic Soft Scaffolds of DA_n

With the excellent stability of macroscopic soft scaffolds **DA_n**, and the obvious supramolecular transformations at microscopic length-scale, a **DA_{11}** macroscopic soft scaffold prepared into a shallow pool of calcium chloride solution was monitored under optical microscopy. At start (0 min) of white-light irradiation, the **DA_{11}** macroscopic soft scaffold showed a deep-blue string with diameter ~ 240 μm (Figure 5a and Movie S1). In the white-light irradiation process, the **DA_{11}** macroscopic soft scaffold was weakened and shrunken. After 60 min irradiation, the **DA_{11}** macroscopic soft scaffold was partially disassembled (Figure 5b), which is consistent to that of observed in **DA_{10}** macroscopic soft scaffold. **DA_7** and **DA_6** macroscopic soft scaffolds were prepared and monitored with the identical method to show deep-blue strings with diameter ~ 500 μm and ~ 570 μm, respectively (Figure 5c, 5e and Movies S2, S3). After 60 min white-light irradiation, both **DA_7** and **DA_6** macroscopic soft scaffolds were significantly disassembled with obvious deep-blue color fading (Figure 5d, 5f). The results indicated that **DA_n** macroscopic soft scaffolds enable photocontrolled disassembly process across multiple length-scale.

DA_n macroscopic soft scaffolds were freshly prepared aqueous solutions of **DA_n** (5.0 wt.%) on a bio-inert glass-bottom petri dish by a shear-flow method, rinsed with PBS, and incubated with human bone marrow-derived mesenchymal stem cells (hBM-MSCs) under conditions of 37 °C with 5% CO_2 for 3 days. **DA_{11}** macroscopic soft scaffold remained intact after incubation at 37 °C, while hBM-MSCs cells grew and attached onto the scaffold surface (Figure 6a–6b). Besides, the macroscopic soft scaffolds of **DA_{10}**, **DA_7**, and **DA_6**, prepared from the identical method, also showed intact macroscopic structure over 3 days 37 °C incubation and hBM-MSCs cells attached onto the scaffold surfaces (Figure 6c–6h). Though the coverage of hBM-MSCs cells onto surfaces of **DA_n** macroscopic soft scaffolds were limited, good cellular

compatibility of **DA$_n$** macroscopic soft scaffolds with hBM-MSCs cells. The current biocompatibility results of **DA$_n$** macroscopic soft scaffolds were the first example to show the intrinsic cytocompatibility of macroscopic soft scaffolds prepared from DA.

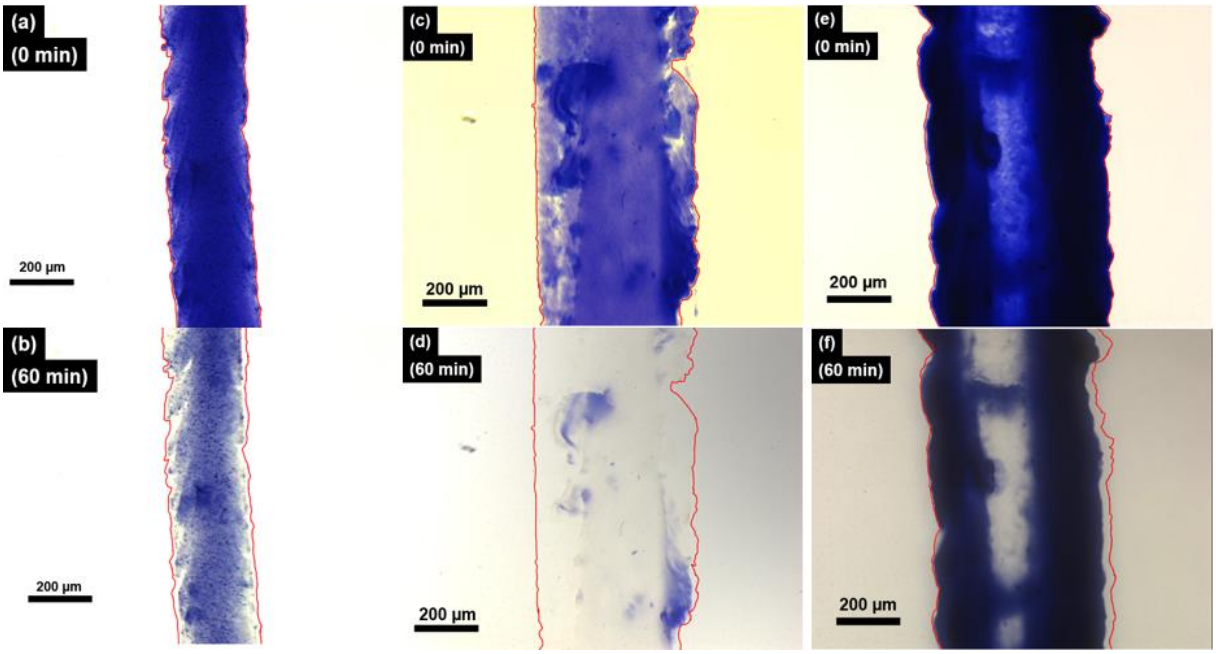

Figure 5. Photographs of a macroscopic soft scaffold were prepared from aqueous solution of (a) **DA$_{11}$** (32.9 mM), (c) **DA$_7$** (36.2 mM), (e) **DA$_6$** (37.2 mM) in $CaCl_2$ solution (150 mM) before white-light irradiation, (b) **DA$_{11}$**, (d) **DA$_7$**, (f) **DA$_6$** after white-light irradiation for 60 min.

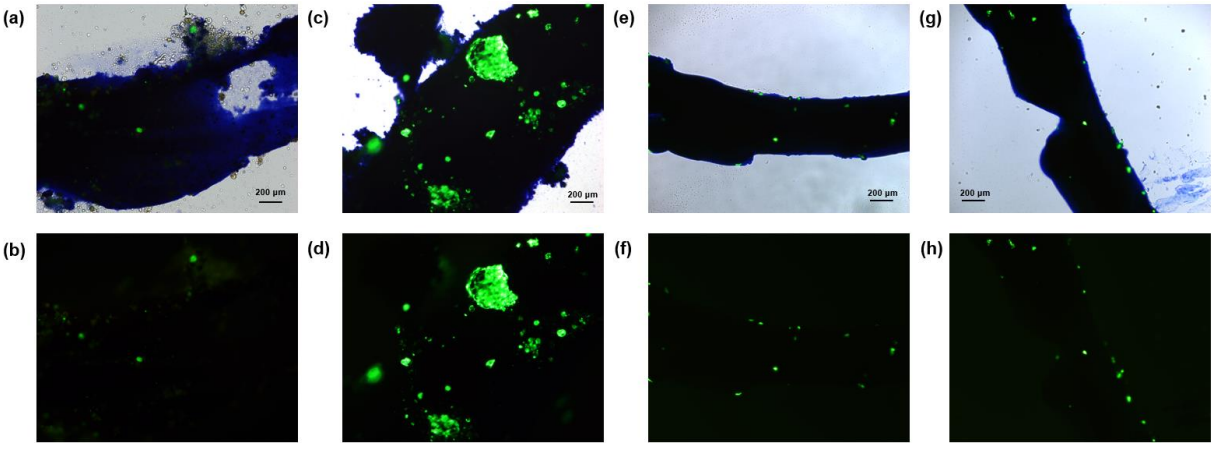

Figure 6. The macroscopic soft scaffold of **DAs** fabricated by shear-flow method. The images were taken by fluorescence microscopy, Photograph of freshly prepared (a) **DA$_{11}$** (c) **DA$_{10}$**, (e) **DA$_7$**, (g) **DA$_6$** merged image of bright field and fluorescence with human mesenchymal stem cells after 3 days of incubation. The fluorescence images of live cells in (b) **DA$_{11}$** (d) **DA$_{10}$**, (f)

DA$_7$, (h) **DA$_6$**, after 3 days of incubation to observe the cell affinity on the hydrogel surface. Scale bar: 200 μm, applied for all panels.

Conclusion

Amphiphilic DASA were synthesized with different chain length of the alkyl-linker in connecting carboxylic acid end-group. Photochemical properties of **DA$_n$** were investigated in both organic and aqueous media with good photoswitchabilities in organic media, while thermal back reactions were hindered in aqueous media. The supramolecular assemblies of **DA$_n$** were observed with large aspect-ratio nanostructures, *i.e.*, nanofibers, in aqueous media, enabling supramolecular transformations upon white-light irradiation. The good stability of supramolecular nanostructure of **DA$_n$** enabled fabrications of macroscopic soft scaffolds with limited unidirectional alignment of the supramolecular nanostructure in scaffolds. The obtained **DA$_n$** macroscopic soft scaffolds showed photoresponsiveness in weakening and disassembling of the scaffolds partially within 60 min photoirradiation. The **DA$_n$** macroscopic soft scaffolds were further incubated with hBM-MSCs cells for 3 days, revealing cell attachment onto the surface of the **DA$_n$** macroscopic soft scaffolds. The limited cytotoxicity and good stability of **DA$_n$** macroscopic soft scaffolds enabled the potential application of current system as cell-material interface and even offered opportunity in fabricating biomedical materials with visible-light controlled microenvironment and future soft robotic systems.

Experimental

Materials

All commercial reagents are purchased from Acros Organics, Aladdin, Alfa Aesar, Bidepharm, Dieckmann, Macklin, Sigma Aldrich and Tokyo Chemical Industry Co. Ltd, and were used as received unless otherwise specified. All reactions were performed under nitrogen unless otherwise specified. Analytical thin layer chromatography (TLC) was performed with

Macherey-Nagel Silica gel 60 UV254 aluminum plates and visualization was accomplished by UV light (254 / 365 nm) or staining with phosphomolybdic acid followed by heating. Flash column chromatography was performed using Macherey-Nagel Silica gel 60 (230–400 mesh). Deuterated solvents were purchased from Cambridge Isotope Laboratories Inc.

UV-Vis Spectroscopy

UV-vis measurements were performed on Agilent Cary 60 UV-Visible Spectrophotometer with a 1 cm path length quartz cuvette. A Luma 40 / Cary 60 temperature-controlled cuvette holder with four optical ports was mounted in the sample compartment of Agilent Cary 60 UV-Visible Spectrophotometer. Irradiation of UV-vis samples were carried out at 20 °C using Thorlabs model M625F2 high-power LED (625 nm, 1.0 A) and a light guide equipped BBZM-I xenon light source (380–800 nm, 300 W) positioned at a distance of 1 cm from the sample.

Preparation of Aqueous Sample

All aqueous solutions of **DA_n** were prepared according to this general procedure. **DA_n** (5.0 wt.%) was mixed with 1.0 equivalent of NaOH in MilliQ water. The obtained aqueous solution of **DA_n** was sonicated for 10 min at room temperature to afford a deep purple solution. The obtained solutions of **DA_n** were directly used or diluted for microscopic and spectroscopic measurements.

Transmission Electron Microscopy (TEM)

TEM was performed on a JEOL Model JEM-2010 Transmission Electron Microscope with hair pin type tungsten filament operating at 120 kV equipped with Gatan 794 CCD camera. TEM samples were prepared by depositing sample solutions (5.0 μL) onto a carbon grid (Micro to Nano, EMR Carbon support film on copper, 400 square mesh) for 20 s. The sample solution was removed by blotting and UranyLess EM stain solution (Electron Microscopy Science, 5.0 μL) was directly deposited onto the grid for 20 s and the stain was removed by blotting.

Scanning Electron Microscopy (SEM) and Polarized Optical Microscopy Analysis

Polarized optical microscopy (POM) was performed on a Leica DM2700-P optical polarizing microscope. Scanning electron microscopy (SEM) was performed on a Tescan VEGA3 Scanning Electron Microscope. Preparation of a soft scaffold composed of **DA$_6$**, **DA$_7$**, **DA$_{11}$** on a glass substrate: When an aqueous solution of **DA$_6$** (5.0 wt.%, 92.9 mM), **DA$_7$** (5.0 wt.%, 90.5 mM), **DA$_{11}$** (5.0 wt.%, 82.2 mM), were manually drawn into an aqueous solution of $CaCl_2$ (150 mM) from a pipette, a noodle-like soft scaffold with an arbitrary length was formed. After removal of the solution of metal chloride, the soft scaffold was washed with MilliQ water (three times), the resulting soft scaffold was used directly for POM experiments. A soft scaffold for SEM was directly prepared on conductive carbon adhesive carbon tape and dried in air for 48 hr before measurement.

Static Light Scattering

The scattering intensities of the samples were determined by static light scattering measurement on a Wyatt Technology DynaPro NanoStar. The scattering intensities were recorded as a parameter for assembly size, since the objects in solutions are anisotropic and the models used by Wyatt software are fitting for spherical objects. To determine the critical aggregation concentration (CAC) of **DA$_6$**, **DA$_7$** and **DA$_{11}$**, the scattering intensities of the solutions of **DA$_6$** (concentration: 1.0×10^{-4} to 0.5 mM), **DA$_7$** (concentration: 1.0×10^{-4} to 0.5 mM) and **DA$_{11}$** (concentration: 1.0×10^{-4} to 0.1 mM) were recorded at 20 °C. This scattering rate was normalized by the concentration of the solution to yield the molar scattering intensities (in M Counts s^{-1} M^{-1}). Ten replications were performed and the data was averaged to show the molar scattering intensity and its error standard deviation.

Wide-Angle X-ray Diffraction

Wide-angle X-ray diffraction (WAXD) of a soft scaffold composed of **DAs** were measured on a sapphire substrate (φ = 2.0 cm) using the Rigaku NANOPIX equipped with a HyPix-6000 (Rigaku) detector. The scattering vector ($q = 4\pi\sin\theta/\lambda$), scattering angle θ and the position of the incident X-ray beam on the detectors were calibrated using several orders of layer reflections from silver behenate (d = 58.380 Å), where λ refers to the wavelength of the X-ray beam (Cu Kα, 1.54 Å). The sample-to-detector distance was ca. 100 mm for WAXD. The obtained diffraction patterns were integrated along the Debye Scherrer ring to afford 1D intensity data using the Rigaku 2DP software.

Cell Attachment Experiment of h-MSCs on **DA_n** Macroscopic Scaffold at Multi-Length Scale

By following standardized preparation protocol of macroscopic scaffold as mentioned above, **DA_n** (5.0 wt.%) aqueous solution was manually drawn into calcium chloride solution (150 mM) in a bioinert surface dish to form macroscopic scaffold. After removing the calcium chloride solution, the obtained macroscopic scaffold was washed with Milli-Q water for three times and added growth medium (0.5 mL) consisting minimum essential medium (MEM Alpha, no phenol red, Gibco, USA), 10 % fetal bovine serum (FBS, Gibco, USA) and 1 % antibiotic–antimycotic (Gibco, USA). Human bone marrow-derived mesenchymal stem cells (h-MSCs, purchased from Lonza) were added into the culture dish and cultured for 3 days under 37 °C and 5 % CO_2 atmosphere. After incubation, the cell-attached **DA_n** macroscopic scaffold was used directly for fluorescent microscopy measurement.

Acknowledgements

This work was supported financially by the National Natural Science Foundation of China (22001223), the Hong Kong Research Grants Council, General Research Fund (GRF 15300521 and GRF 15305822), Croucher Foundation (Croucher Innovation Award 2021), the Hong Kong Special Administrative Region Government (InnoHK), the Hong Kong Polytechnic University (W08A, ZVST) for F. K-C. L., JSPS KAKENHI (JP21K04877) and the CREST, Japan Science and Technology Agency (JPMJCR23L2) for T.K.. We acknowledge the technical support from UCEA and ULS of PolyU. All authors appreciate sincerely to Prof. Dr. Takanori Fukushima (Laboratory for Chemistry and Life Science, Institute of Innovative Research, Tokyo Institute of Technology) for his generous support and help in X-ray diffraction measurements and helpful suggestions.

References

1. Zhang, J.; Zou, Q.; Tian, H. *Adv. Mater.* **2013**, *25* (3), 378-399.
2. Feringa, B. L. *Molecular Switches*; 2001.
3. Wang, Z.; Erhart, P.; Li, T.; Zhang, Z.-Y.; Sampedro, D.; Hu, Z.; Wegner, H. A.; Brummel, O.; Libuda, J.; Nielsen, M. B.; Moth-Poulsen, K. *Joule* **2021**, *5* (12), 3116-3136.
4. Pham, T. C.; Nguyen, V.-N.; Choi, Y.; Lee, S.; Yoon, J. *Chem. Rev.* **2021**, *121* (21), 13454-13619.
5. Kinbara, K.; Aida, T. *Chem. Rev.* **2005**, *105* (4), 1377-1400.
6. Chapman, D. *Quarterly Reviews of Biophysics* **1975**, *8* (2), 185-235.
7. Cooper, R. A. *Journal of Supramolecular Structure* **1978**, *8* (4), 413-430.
8. Wehrle-Haller, B.; Imhof, B. A. *The International Journal of Biochemistry & Cell Biology* **2003**, *35* (1), 39-50.
9. Wang, C.; Wang, S.; Yang, H.; Xiang, Y.; Wang, X.; Bao, C.; Zhu, L.; Tian, H.; Qu, D. H. *Angew. Chem. Int. Ed.* **2021**, *60* (27), 14836-14840.
10. Wang, Q.; Zhang, Q.; Zhang, Q. W.; Li, X.; Zhao, C. X.; Xu, T. Y.; Qu, D. H.; Tian, H. *Nat. Commun.* **2020**, *11* (1), 158.
11. Qu, D. H.; Wang, Q. C.; Zhang, Q. W.; Ma, X.; Tian, H. *Chem. Rev.* **2015**, *115* (15), 7543-88.
12. Royes, J.; Bjornestad, V. A.; Brun, G.; Narayanan, T.; Lund, R.; Tribet, C. *J. Colloid Interface Sci.* **2022**, *610*, 830-841.
13. Shi, Z. T.; Hu, Y. X.; Hu, Z.; Zhang, Q.; Chen, S. Y.; Chen, M.; Yu, J. J.; Yin, G. Q.; Sun, H.; Xu, L.; Li, X.; Feringa, B. L.; Yang, H. B.; Tian, H.; Qu, D. H. *J. Am. Chem. Soc.* **2021**, *143* (1), 442-452.
14. Sun, H. L.; Chen, Y.; Han, X.; Liu, Y. *Angew. Chem. Int. Ed.* **2017**, *56* (25), 7062-7065.
15. Aida, T.; Meijer, E. W.; Stupp, S. I. *Science* **2012**, *335* (6070), 813-817.
16. Krieg, E.; Bastings, M. M. C.; Besenius, P.; Rybtchinski, B. *Chem. Rev.* **2016**, *116* (4), 2414-2477.
17. Chen, S.; Costil, R.; Leung, F. K.; Feringa, B. L. *Angew. Chem. Int. Ed.* **2021**, *60* (21), 11604-11627.
18. Lubbe, A. S.; van Leeuwen, T.; Wezenberg, S. J.; Feringa, B. L. *Tetrahedron* **2017**, *73* (33), 4837-4848.
19. Feringa, B. L. *Angew. Chem. Int. Ed.* **2017**, *56* (37), 11060-11078.
20. Leung, F. K.-C. Aqueous Supramolecular Assemblies of Photocontrolled Molecular Amphiphiles. In *Supramolecular Assemblies Based on Electrostatic Interactions*; 2022; pp 267-308.
21. Cautela, J.; Stenqvist, B.; Schillén, K.; Belić, D.; Månsson, L. K.; Hagemans, F.; Seuss, M.; Fery, A.; Crassous, J. J.; Galantini, L. *ACS Nano* **2020**, *14* (11), 15748-15756.
22. Fukino, T.; Joo, H.; Hisada, Y.; Obana, M.; Yamagishi, H.; Hikima, T.; Takata, M.; Fujita, N.; Aida, T. *Science* **2014**, *344* (6183), 499-504.
23. Chen, S.; Costil, R.; Leung, F. K.; Feringa, B. L. *Angew. Chem. Int. Ed.* **2021**, *60* (21), 11604-11627.
24. Santilli, A.; Lapi, A.; Cautela, J.; D'Abramo, M.; Giuseppe Chen, C.; Del Giudice, A.; Sennato, S.; Belić, D.; Hugo Soto Tellini, V.; Schillén, K.; di Gregorio, M. C.; Galantini, L. *J. Colloid Interface Sci.* **2022**, *623*, 723-734.
25. Volaric, J.; Szymanski, W.; Simeth, N. A.; Feringa, B. L. *Chem. Soc. Rev.* **2021**, *50* (22), 12377-12449.

26. Costil, R.; Holzheimer, M.; Crespi, S.; Simeth, N. A.; Feringa, B. L. *Chem. Rev.* **2021**, *121* (21), 13213-13237.
27. Kwan, K. S.; Lui, Y. Y.; Kajitani, T.; Leung, F. K. *Macromol. Rapid Commun.* **2022**, *43* (21), e2200438.
28. Cheung, L.-H.; Liu, B. B.; Leung, F. K.-C. *Polym. J.* **2023**.
29. Crespi, S.; Simeth, N. A.; König, B. *Nat. Rev. Chem.* **2019**, *3* (3), 133-146.
30. Kassem, S.; van Leeuwen, T.; Lubbe, A. S.; Wilson, M. R.; Feringa, B. L.; Leigh, D. A. *Chem. Soc. Rev.* **2017**, *46* (9), 2592-2621.
31. Baroncini, M.; Silvi, S.; Credi, A. *Chem. Rev.* **2020**, *120* (1), 200-268.
32. Kortekaas, L.; Browne, W. R. *Chem. Soc. Rev.* **2019**, *48* (12), 3406-3424.
33. Klajn, R. *Chem. Soc. Rev.* **2014**, *43* (1), 148-84.
34. Schnurbus, M.; Kabat, M.; Jarek, E.; Krzan, M.; Warszynski, P.; Braunschweig, B. *Langmuir* **2020**, *36* (25), 6871-6879.
35. Yau, J. C.-K.; Hung, K.-L.; Ren, Y.; Kajitani, T.; Stuart, M. C. A.; Leung, F. K.-C. *J. Colloid Interface Sci.* **2024**, *662*, 391-403.
36. Chau, M.-H.; Stuart, M. C. A.; Leung, F. K.-C. *Colloids Surf. A Physicochem. Eng.* **2023**, *661*, 130939.
37. Chau, A. K.-H.; Cheung, L.-H.; Leung, F. K.-C. *Dyes Pigm.* **2022**, *208*.
38. Cheung, L. H.; Kajitani, T.; Leung, F. K. *J. Colloid Interface Sci.* **2022**, *628* (Pt A), 984-993.
39. Dattler, D.; Fuks, G.; Heiser, J.; Moulin, E.; Perrot, A.; Yao, X.; Giuseppone, N. *Chem. Rev.* **2020**, *120* (1), 310-433.
40. Goulet-Hanssens, A.; Eisenreich, F.; Hecht, S. *Adv. Mater.* **2020**, *32* (20), e1905966.
41. Zhang, Q.; Qu, D. H.; Tian, H. *Adv. Opt. Mater.* **2019**, *7* (16), 1900033.
42. Leung, F. K.; van den Enk, T.; Kajitani, T.; Chen, J.; Stuart, M. C. A.; Kuipers, J.; Fukushima, T.; Feringa, B. L. *J. Am. Chem. Soc.* **2018**, *140* (50), 17724-17733.
43. Leung, F. K.; Kajitani, T.; Stuart, M. C. A.; Fukushima, T.; Feringa, B. L. *Angew. Chem. Int. Ed.* **2019**, *58* (32), 10985-10989.
44. Chen, J.; Leung, F. K.; Stuart, M. C. A.; Kajitani, T.; Fukushima, T.; van der Giessen, E.; Feringa, B. L. *Nat. Chem.* **2018**, *10* (2), 132-138.
45. Chau, A. K.; Leung, F. K. *Adv. Colloid Interface Sci.* **2023**, *315*, 102892.
46. Li, C.; Iscen, A.; Palmer, L. C.; Schatz, G. C.; Stupp, S. I. *Journal of the American Chemical Society* **2020**, *142* (18), 8447-8453.
47. Fuentes, E.; Gerth, M.; Berrocal, J. A.; Matera, C.; Gorostiza, P.; Voets, I. K.; Pujals, S.; Albertazzi, L. *Journal of the American Chemical Society* **2020**, *142* (22), 10069-10078.
48. Helmy, S.; Oh, S.; Leibfarth, F. A.; Hawker, C. J.; Read de Alaniz, J. *The Journal of Organic Chemistry* **2014**, *79* (23), 11316-11329.
49. Helmy, S.; Leibfarth, F. A.; Oh, S.; Poelma, J. E.; Hawker, C. J.; Read de Alaniz, J. *Journal of the American Chemical Society* **2014**, *136* (23), 8169-8172.
50. Mao, L.; Wang, Z.; Duan, Y.; Xiong, C.; He, C.; Deng, X.; Zheng, Y.; Wang, D. *ACS Nano* **2021**, *15* (6), 10384-10392.
51. Clerc, M.; Stricker, F.; Ulrich, S.; Sroda, M.; Bruns, N.; Boesel, L. F.; Read de Alaniz, J. *Angew. Chem. Int. Ed.* **2021**, *60* (18), 10219-10227.
52. Poelma, S. O.; Oh, S. S.; Helmy, S.; Knight, A. S.; Burnett, G. L.; Soh, H. T.; Hawker, C. J.; Read de Alaniz, J. *Chem. Commun.* **2016**, *52* (69), 10525-8.
53. Berraud-Pache, R.; Santamaría-Aranda, E.; de Souza, B.; Bistoni, G.; Neese, F.; Sampedro, D.; Izsák, R. *Chemical Science* **2021**, *12* (8), 2916-2924, 10.1039/D0SC06575G.

54. Saha, R.; Devaraj, A.; Bhattacharyya, S.; Das, S.; Zangrando, E.; Mukherjee, P. S. *Journal of the American Chemical Society* **2019**, *141* (21), 8638-8645.
55. Yang, S.; Liu, J.; Cao, Z.; Li, M.; Luo, Q.; Qu, D. *Dyes Pigm.* **2018**, *148*, 341-347.
56. Senthilkumar, T.; Zhou, L.; Gu, Q.; Liu, L.; Lv, F.; Wang, S. *Angew. Chem. Int. Ed.* **2018**, *57* (40), 13114-13119.
57. Mallo, N.; Foley, E. D.; Iranmanesh, H.; Kennedy, A. D. W.; Luis, E. T.; Ho, J.; Harper, J. B.; Beves, J. E. *Chemical Science* **2018**, *9* (43), 8242-8252.
58. Rifaie-Graham, O.; Ulrich, S.; Galensowske, N. F. B.; Balog, S.; Chami, M.; Rentsch, D.; Hemmer, J. R.; Read de Alaniz, J.; Boesel, L. F.; Bruns, N. *Journal of the American Chemical Society* **2018**, *140* (25), 8027-8036.
59. Hemmer, J. R.; Page, Z. A.; Clark, K. D.; Stricker, F.; Dolinski, N. D.; Hawker, C. J.; Read de Alaniz, J. *Journal of the American Chemical Society* **2018**, *140* (33), 10425-10429.
60. Hemmer, J. R.; Poelma, S. O.; Treat, N.; Page, Z. A.; Dolinski, N. D.; Diaz, Y. J.; Tomlinson, W.; Clark, K. D.; Hooper, J. P.; Hawker, C.; Read de Alaniz, J. *Journal of the American Chemical Society* **2016**, *138* (42), 13960-13966.
61. Lerch, M. M.; Wezenberg, S. J.; Szymanski, W.; Feringa, B. L. *Journal of the American Chemical Society* **2016**, *138* (20), 6344-6347.